Multiple Time Scale Chaos in a Schmitt Trigger Circuit

Thomas L Carroll
Code 6362, US Naval Research Lab

Abstract-- It is known that stray rf signals can produce nonlinear effects that disrupt the operation of the circuits, but the mechanisms by which this disruption occurs are not well known. In this paper, an emitter coupled Schmitt trigger circuit is driven with a high frequency signal to look for disruptive effects. As the circuit makes a transition between mode locked states (period 2 and period 3 for example), there is a region of chaos in which the largest peak in the power spectrum is in between the mode locked frequencies, and is not related to the driving frequency by an integer multiple. This chaos resembles the chaos seen during a period adding sequence, except that it contains frequencies ranging over many orders of magnitude, from the driving frequencies on the order of megahertz, down to a few hertz. It is found that only a one transistor circuit is necessary to produce this extremely broad band chaos, and true quasiperiodicity is not seen in this circuit. The single transistor circuit is then simulated to confirm the frequency conversion effects.

PACS 05.45.+a, 84.30.Sk

It has been discovered mostly through trial and error that electronic circuits, even those operating in the audio frequency range, can be adversely affected by radiofrequency (rf) interference. In digital circuits, it is believed that pn junctions in the circuit act as diodes to rectify the rf signal, producing a relatively constant (dc) offset that was not anticipated by the circuit designer. One way in which this dc offset can disrupt circuit operation is to shift the level at

which a digital circuit shifts between the 1 and 0 states, causing a bit error.

There are other mechanisms besides rectification by which an rf signal can cause low frequency interference, but these have not been thoroughly studied. If a circuit has multiple stable states, the circuit can either spontaneously switch between these states, or be forced to switch between them by an external rf signal. These effects can result in a changing dc signal, which can disrupt circuit operation. In this paper, I consider a different mechanism- very broad band chaos. As the rf driven circuit makes a transition between 2 states of different periodicities (period 2 to period 3, for example), there is an intermediate chaotic state whose power spectrum is very broad band, reaching down to very low frequencies. If I generate a time series by strobing the circuit output with the drive signal, I see that in this chaotic state, the peak frequency in the strobed time series signal is related to the driving frequency by a number that may be irrational.

Introduction

It has been known for many years that stray rf signals can disrupt the operation of some electronic circuits [1]. In much of the work to date, an electronic system is exposed to rf radiation to see if disruption occurs. Statistical analysis is common, but usually only the simplest physical effects, such as thermal damage, or rectification of the rf signal, are considered [1]. Existing theory is aimed mostly at predicting the levels of electromagnetic fields in enclosures, while the mechanisms by which circuits may be damaged or disrupted is usually discovered by experiment only.

It is currently believed by many in the high power microwave community that intentional electromagnetic interference is an increasing threat [1]. Terrorists, criminals, or combatants may focus high power microwave beams on targeted electronic systems. With this intentional interference, the electromagnetic field levels could be much higher than the levels seen from unintentional stray fields only.

In order to better understand the physical mechanisms that lead to disruption, I study circuits with only a few pn junctions. A single pn junction, when combined with an inductor, forms the much studied diode resonator [2-8], which can produce period doubling and chaos. The diode resonator has a resonance at a frequency $1/\left(2\pi\sqrt{LC}\right)$, where C is the diode capacitance and L is the value of the inductor. At rf frequencies on the order of 1 GHz, the inductance L may be provided by the circuit wiring alone, so the presence of pn junctions may cause unexpected high frequency resonances in a circuit, leading to nonlinear effects.

A single diode resonator can produce period doubling and chaos, but it does not produce signals with frequencies more than an order of magnitude lower than the rf driving signal. In order to produce low frequencies, a circuit more complicated than a single diode resonator is necessary.

In previous work, it was shown that some transistor circuits may have regions of multistable behavior. It was shown in a single transistor amplifier that the presence of a large capacitor caused the amplifier to

slowly switch between 2 different states [9, 10], producing a dc signal with a frequency 6 orders of magnitude lower than the rf signal that drove the amplifier. In another paper, bistability was demonstrated in a digital CMOS inverter circuit [11]. Sweeping the rf frequency across the bistable region could produce a low frequency signal.

In this paper, I study a simple circuit that produces low frequency signals without multistability. Previous work with coupled arrays of diode resonators suggested that circuits similar to these coupled arrays might produce complex signals, such as quasiperiodicity [12, 13]. In particular, an emitter coupled Schmitt trigger circuit, which uses 2 transistors, resembles a coupled diode array.

Schmitt Trigger

A Schmitt trigger is used to convert a time varying signal into a square wave between 0 and 5 V, usually so that the signal can be used as an input to a digital system [14]. Figure 1 is a schematic of one type of Schmitt trigger, an emitter coupled Schmitt trigger.

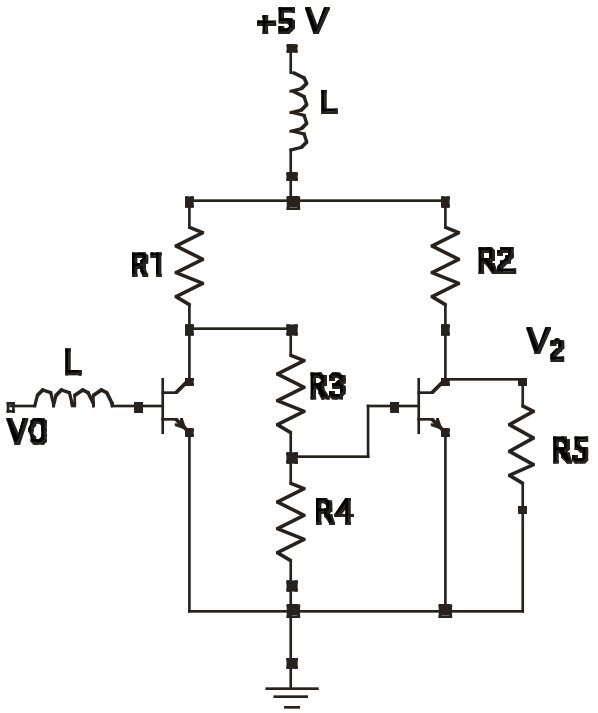

Fig. 1. Emitter coupled Schmitt trigger. *L* = 100 mH, *R1=R2=R3=R4= R5*=1 kΩ.

Both transistors are type 2n2222.

In fig. 1, 2 inductors have been added to the circuit to reduce the resonant frequency of the diode resonator part of the circuit. Normally these frequencies are on the order of GHz, but digitizing at these frequencies is expensive, so the inductors are used to shift the resonance to a lower frequency. There may also be other effects at high frequencies, such as stray capacitances, or inductance in the resistors, and the actual inductance of the wires may not be known precisely, so shifting the resonance to a lower frequency also allows the circuit to be better characterized.

The Schmitt trigger circuit was driven with a sinusoidal signal $V_0 = A_0 sin(\omega t) + B_0$, where the frequency ranged from 500 kHz to 8 MHz, and amplitudes from 0.5 V to 5 V. The driving signal was applied at the point marked V_0 in fig. 1, and the response of the circuit was measured at the point marked V_2. The circuit response was complicated, but period doubling, chaos, and low frequency effects were seen. Figure 2 shows 2

typical time series signals from the Schmitt trigger circuit that show low frequency behavior.

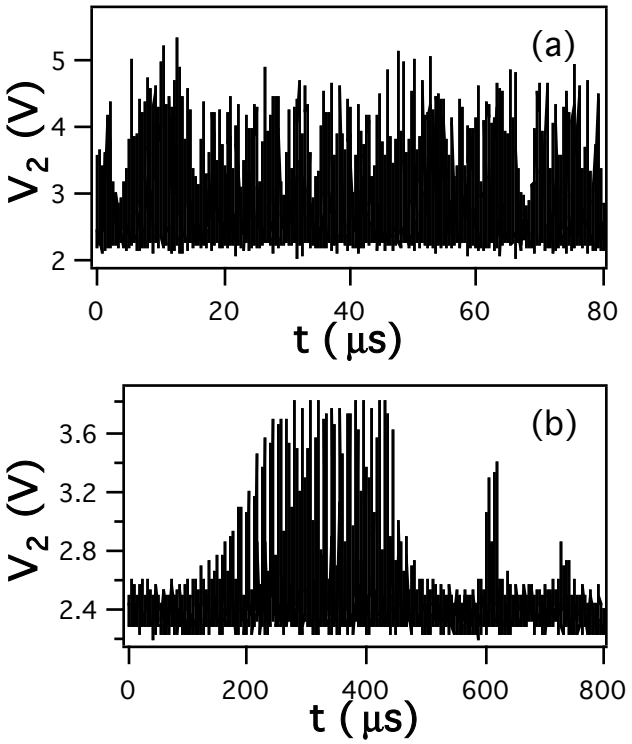

Fig. 2. Time series of V_{out} measured from the Schmitt trigger circuit. In (a), the amplitude of the driving signal V_0 was 5 V, and the frequency was 5.3 MHz. In (b), V_0 had an amplitude of 1 V and a frequency of 510 kHz.

In fig 2(a), the amplitude of the output signal varies irregularly. This irregular variation appears as a low frequency signal. In (b), irregular bursting is seen. Both of these low frequency effects produced broad band behavior in which most of the energy was below 10 kHz. This type of low frequency behavior was not seen in a single diode resonator circuit.

The parameter regions for which low frequency effects were seen are plotted in Figure 3. The signal V_2 was filtered with a low pass filter with a break frequency of 10 kHz, and the rms amplitude of the filter output was measured for different amplitudes and frequencies of the driving signal V_0.

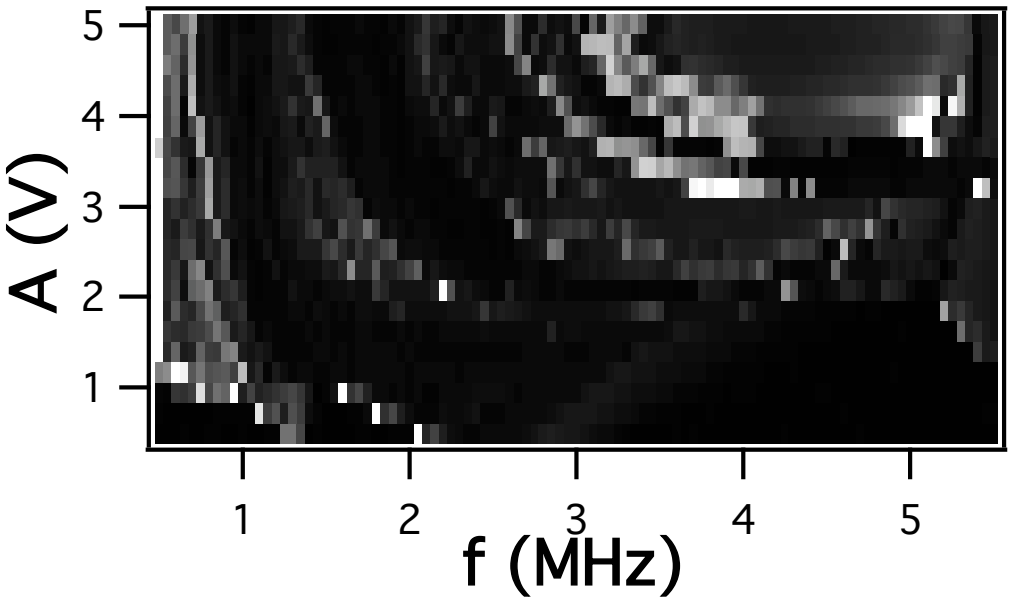

Figure 3. RMS amplitude of the low pass filtered output signal from the Schmitt trigger circuit, for different driving amplitudes (A_0) and frequencies. The largest values are white, while the smallest values are black.

As fig. 3 shows, low frequency behavior occurs for several different parameter regions in the Schmitt trigger circuit. This particular circuit is difficult to analyze, since each inductor and each capacitor (2 internal capacitances per transistor) contributes a dynamical variable, making the Schmitt trigger a 6 dimensional system. Analysis is simpler if parts of the circuit that do not contribute to the low frequency behavior are removed, so that the origin of this behavior is easier to understand.

Single Transistor Circuit

When circuit elements are removed from the circuit in fig. 1, it is seen that the same type of low frequency behavior seen in the full circuit

can be produced by a circuit with only a single transistor, shown in Figure 4.

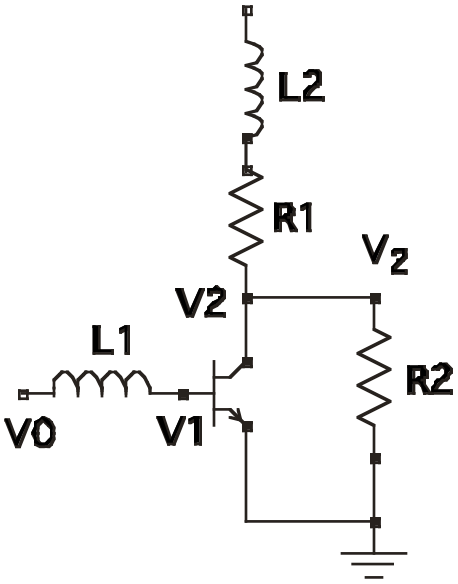

Fig 4. Single transistor circuit that shows low frequency behavior. *L1* = *L2* = 100 mH, *R1* = 1 kΩ, *R2* = 2 kΩ. V_2 shows the location of the output voltage, while V_0 is the location where the rf signal was applied.

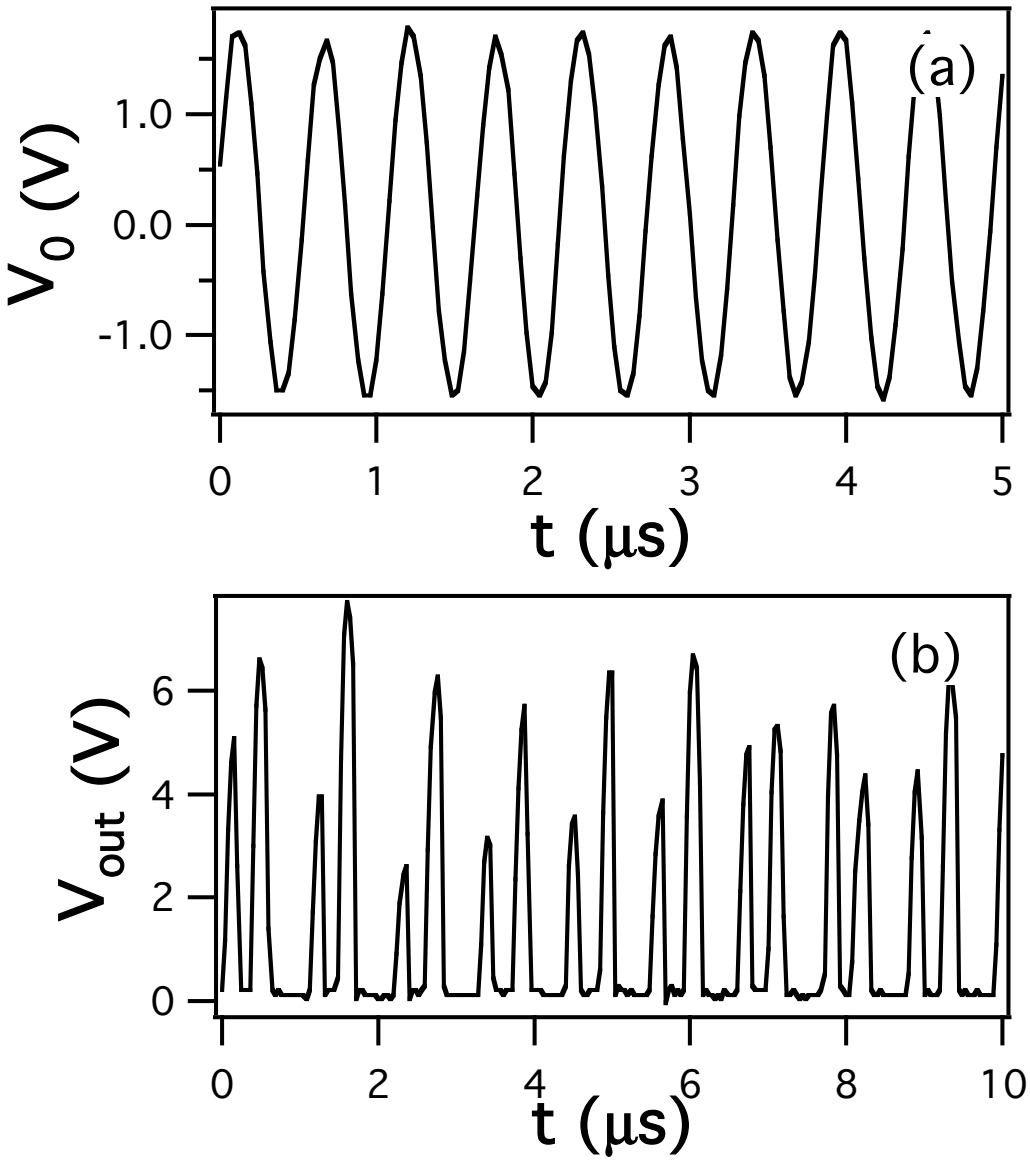

Fig. 5. Output from the single transistor circuit, when the driving amplitude was 2.5 V and the driving frequency was 1.82 MHz. (a) is the driving signal, and (b) is the output signal.

Figure 5 shows a typical output signal from the single transistor circuit. While the output signal in fig. 5 roughly resembles a period doubled signal, the amplitude varies irregularly, suggesting that it may be quasiperiodic or chaotic. This irregular variation produces a low frequency signal.

Figure 6 compares the low frequency part of the power spectra of the output signal from the single transistor circuit for 2 different driving frequencies. In 6(a), which shows low frequency behavior, the driving amplitude was 1.0 V and the frequency was 2.8 MHz. In 6(b), in which no low frequency behavior was seen, the drive amplitude was also 1.0 V, with a frequency of 2.3 MHz.

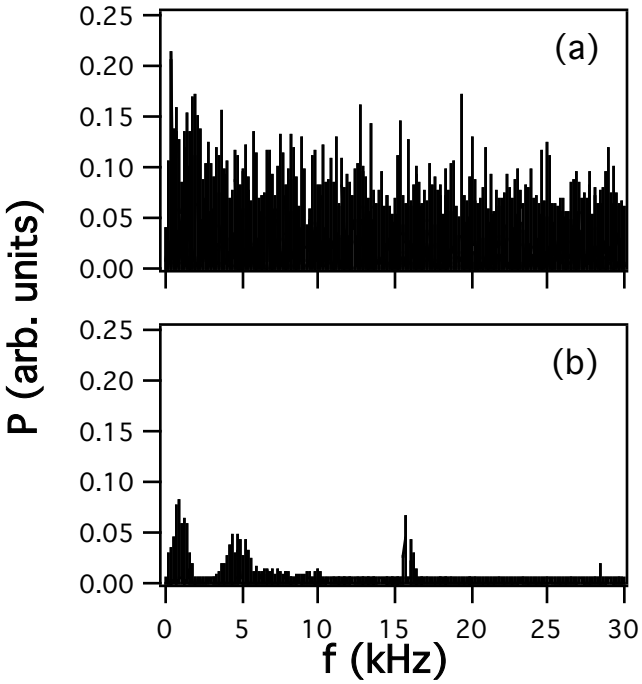

Fig 6. (a) Low frequency power spectrum of the output from the single transistor circuit with a driving amplitude of 1 V and a frequency of 2.8 MHz. (b) The same

for a driving frequency of 2.3 MHz. The structure seen in (b) all occurs at multiples of 60 Hz, so it is most likely interference picked up in the electronics after the single transistor circuit.

The signals in fig. (6) were passed through a low pass filter to eliminate aliasing problems that would be caused by sampling a high frequency signal at a slow rate (60,000 samples/sec in this case). The filter was isolated from the single transistor circuit by a 1 MΩ resistor, so the signal amplitude has been reduced. The spectrum in fig 6(b) does show some structure, but this was caused by 60 Hz interference.

The amplitude at any one frequency in the low frequency spectrum in 6(a) is not large, but the low frequencies cover a broad band, so the total power in the low frequency signal can be large.

In Figure 7, the regions of low frequency behavior for the single transistor circuit are plotted, again by low pass filtering the output signal V_2 at 10 kHz and measuring the rms amplitude of the low pass signal.

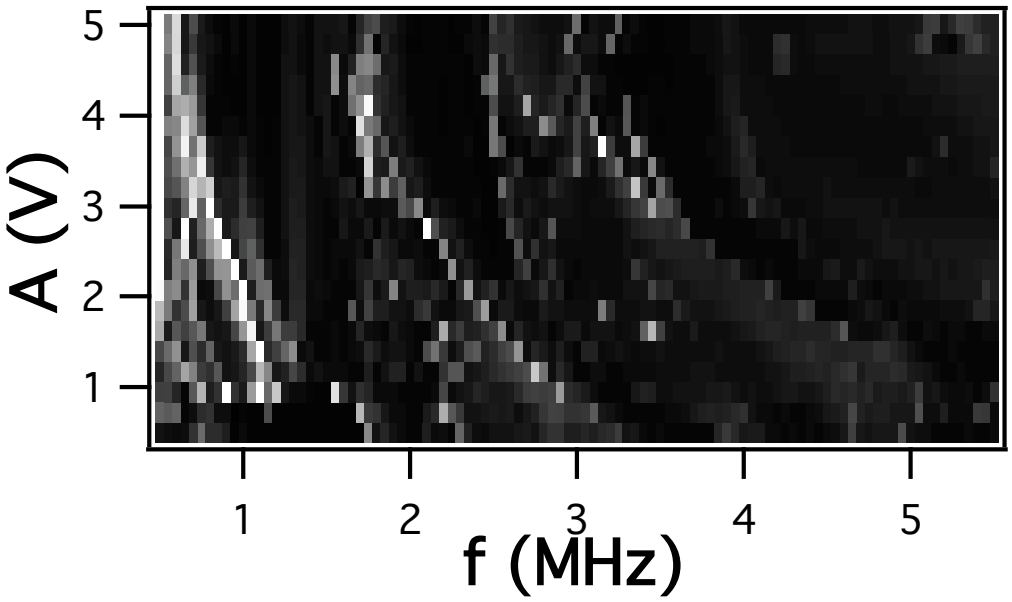

Fig 7. RMS amplitude of the low pass filtered output signal from the single transistor circuit, for different driving amplitudes (A) and frequencies. The largest values are white, while the smallest values are black.

Fig. 7 shows bands of low frequency similar to the bands seen in fig. 3, although the overall scale seems to be shifted to slightly higher frequencies. Figures 6 and 7 show that only one of the transistors in the Schmitt trigger circuit is necessary to produce the low frequency effects.

Simulations

Numerical simulations are useful to understand the origin of the low frequency behavior seen in the circuits and to confirm that some other factor not characterized in the circuit (stray capacitance, for example) is not affecting the observed behavior.

The single transistor circuit was simulated by these 4 differential equations:

$$\begin{aligned}
\frac{dV_1}{dt} &= \frac{-1}{R_1 R_2 C_{be}}\left[R_2 R_2\left(I_c - I_b - I_1 - I_2\right) + R_1 V_2 + 2R_2 V_2\right] \\
\frac{dV_2}{dt} &= \frac{1}{C_{be} C_{cb}}\left[C_{cb}(I_b + I_1) - (C_{be} - C_{cb})\left(I_2 - I_c - V_2 / R_2\right)\right] \\
\frac{dI_1}{dt} &= \frac{1}{L_1}\left(V_0 - V_1\right) \\
\frac{dI_2}{dt} &= \frac{1}{L_2}\left(V_0 + V_a - V_2 - R_1 I_2\right)
\end{aligned} \tag{1}$$

Resistor and inductor values are given in fig. 4. V_1 and V_2 are marked on fig. 4. I_1 is the current through inductor L_1 , and I_2 is the current through inductor L_2 . The currents I_c and I_b are given by the Ebers-Moll equations [15]:

$$I_C = I_0\left[-\left(e^{\frac{-qV_{CB}}{kT}}-1\right)+\alpha\left(e^{\frac{qV_{BE}}{kT}}-1\right)\right]$$
$$I_E = I_0\left[\left(e^{\frac{qV_{BE}}{kT}}-1\right)-\alpha\left(e^{\frac{-qV_{CB}}{kT}}-1\right)\right] \qquad (2)$$
$$I_B = I_E - I_C$$

where I_C is the current flowing into the collector, I_B is the current flowing into the base, and I_E is the current flowing out of the emitter. $V_{CB} = V_2\text{-}V_1$ is the collector-base voltage, $V_{BE} = V_1\text{-}0$ is the base-emitter voltage, q is the charge of 1 electron, k is the Boltzman constant, T is the temperature in Kelvins, and α is the fraction of current that flows from the collector, through the base, and into the emitter (or in the reverse direction). The fraction a is typically just below 1.0: for this simulation, a value of 0.995 was used. The reverse current I_0 was 10^{-9} A, a value obtained from the data sheet for the transistor.

The transistor capacitance was modeled as a sum of a junction capacitance and a diffusion capacitance, where the junction capacitance was given by [16]

$$C_J(V) = \frac{C_J(0)}{\left(\left(V-V_b\right)^2+b\right)^{n/2}}\left(1+\frac{n}{1-n}\frac{b}{\left(\left(V-V_b\right)^2+b\right)}\right) \qquad (3)$$

where V_b is the built-in voltage (approximately the turn on voltage) for the junction, V is the voltage across the junction, and b and n may be estimated by measuring junction capacitance as a function of V for $V < V_b$. There is a common simple expression for the junction capacitance that involves only the inverse of the square root of $V - V_b$ [15], but the simpler expression has a singularity at $V = V_b$, which is not physical and makes the capacitance difficult to evaluate near $V = V_b$. Poon and Gummel [16] derived the phenomenological expression for junction capacitance shown in eq. (3) to closely match the inverse square root low for $V < V_b$, but without the singularity. The factors b and n are found by fitting the measured capacitance vs. voltage curve for the base-emitter junction from

a real transistor. Poon and Gummel realized that for $V > V_b$, the capacitance would be dominated by the diffusion capacitance shown in eq. (4) below, so the specific value of eq. (3) for $V > V_b$ was less important. For these simulations, V_b = 0.66 V, b = 0.09 and n =0.08. The junction capacitance at zero bias voltage was $C_j(0)$ = 17 pF.

The other type of capacitance, the diffusion capacitance, was described by [15]

$$C_D(V) = C_D(0)e^{\left(\frac{qV}{kT}\right)} \tag{4}$$

where $C_D(0)$ = 10^{-18} F.

In the model of eqs. (1-4), the zero bias junction capacitance was set to 17 pF. Using only the base-emitter capacitance, the resonant frequency of the series resonant circuit is $1/\left(2\pi\sqrt{LC}\right)$ = 3.8 MHz. Another possible series resonant circuit is the inductor L_2 (in fig 4) combine with the collector base and base emitter capacitances (which add in series). The resonant frequency of this circuit was 5.46 MHz.

The model of eq. (1-4) was numerically integrated using a 4-th order Runge-Kutta integration routine with a fixed time step. The time step was initially set at 10^{-12} s until all transients died out, at which point it was set to 10^{-10} s.

Figure 8 shows a typical waveform seen in the single transistor simulation.

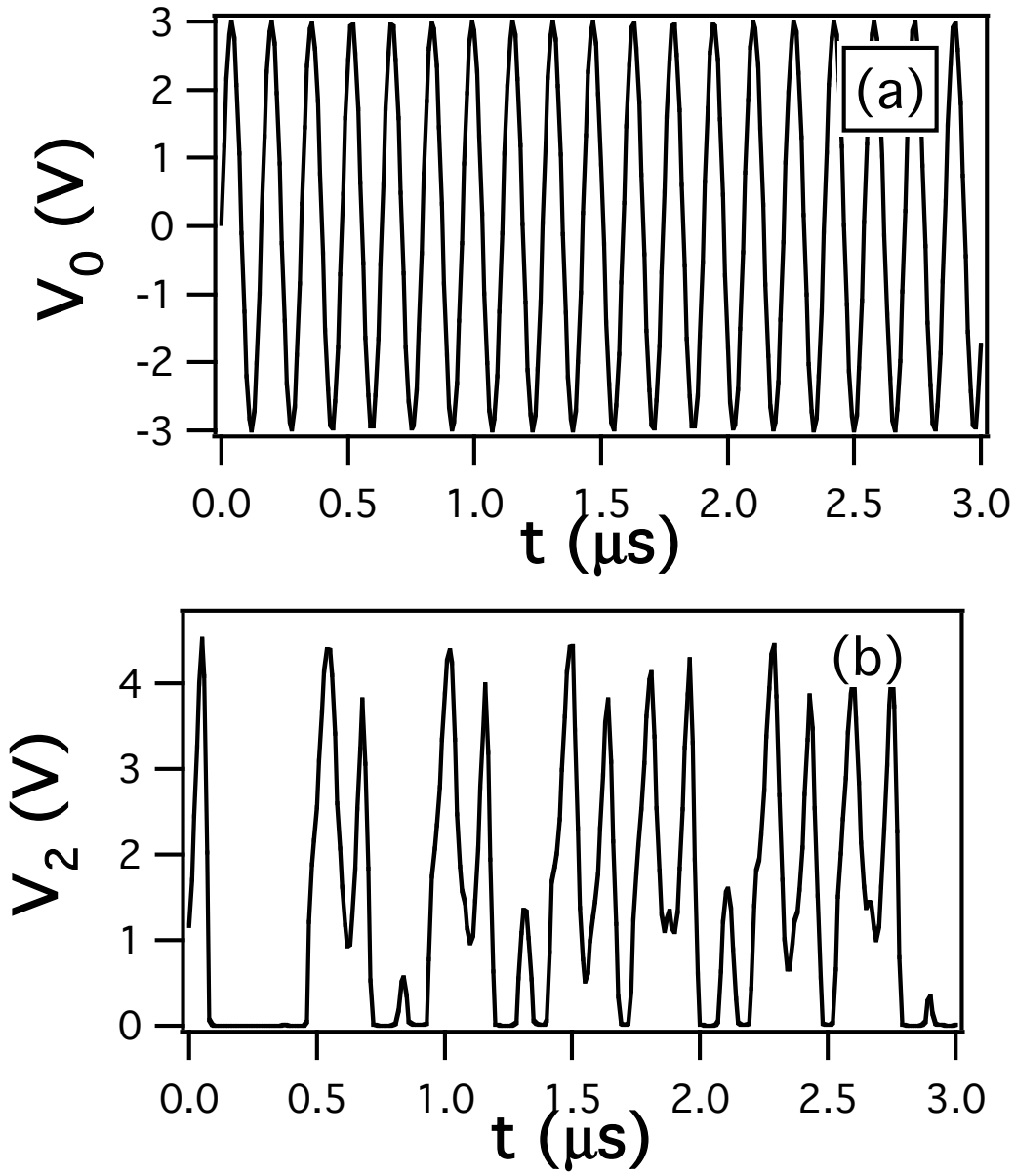

Fig. 8. Time series signals for the single transistor simulation, for a driving amplitude of 3.0 V and a frequency of 6.3 MHz. (a) shows the driving signal, while (b) shows the variable V_2.

The V_2 signal can be seen to resemble the output voltage from the actual transistor circuit plotted in fig. 5. The signal at times resembles a period doubled signal, but the amplitude varies in an irregular fashion.

Figure 9 compares the low frequency part of the power spectra of the output signal from the simulation for 2 different driving frequencies. In 9(a), which shows low frequency behavior, the driving amplitude was 3.0 V and the frequency was 6.3 MHz. The driving power in 9(a) was estimated by multiplying the driving signal V_0 by the current through the inductor L_1, yielding an rms power of 1.3 mW.. Whether or not this power could be achieved by actually irradiating a circuit would depend on such factors as the physical size of the circuit, the power and antenna configuration of the radiating system, its distance, and any shielding of the circuit. In 9(b), in which no low frequency behavior was seen, the drive amplitude was also 3.0 V, with a frequency of 3.0 MHz.

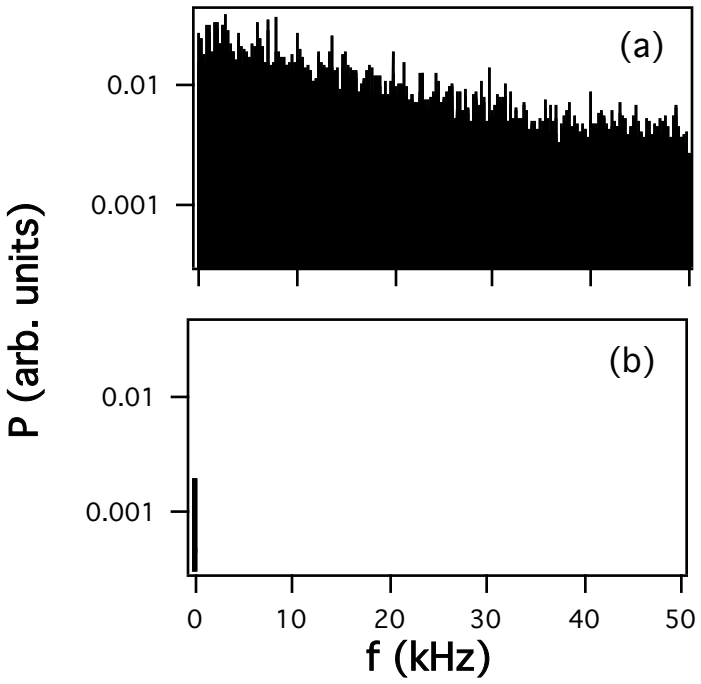

Fig 9. (a) Low frequency power spectrum of the output from the single transistor simulation with a driving amplitude of 3 V and a frequency of 6.3 MHz. (b) The same for a driving frequency of 3.0 MHz.

The signals in fig. (9) were passed through a low pass filter to eliminate aliasing problems that would be caused by sampling a high frequency signal at a slow rate (10^5 samples/sec in this case).

Figure 10 shows the regions of low frequency behavior seen in the simulation of the single transistor circuit. Fig. 10 was produced by low pass filtering the V_2 variable from the simulation and plotting the rms amplitude of the resulting low frequency signal. As in the actual circuit, the low frequency power was spread over a broad band of frequencies.

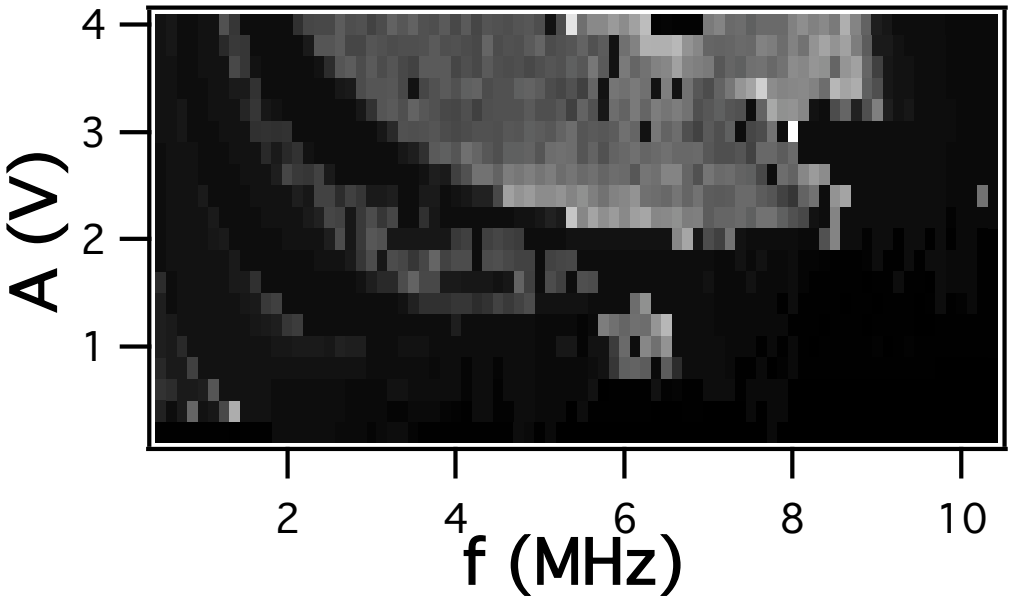

Fig. 10. RMS amplitude of the low pass filtered output signal from the simulation of the single transistor circuit, for different driving amplitudes (A) and frequencies. The largest values are white, while the smallest values are black.

Comparing fig. 10 to fig. 7 from the experiment, the low frequency behavior in the simulation also occurs in discrete bands in parameter space. The bands appear to have some symmetry about 6 MHz, which is close to the resonant frequency of the inductor L_2 combined with the collector base and base emitter capacitances.

Theory

The decision to study a Schmitt trigger circuit was motivated by its similarity to a coupled diode array, which was shown to exhibit quasiperiodicity [13]. Subsequently, it was shown that quasiperiodicity could be a product of symmetrically coupled identical period doubling systems [12]. The single transistor circuit above contains 2 back to back pn junctions (the transistor), each of which is in series with an inductor, so the single transistor circuit resembles 2 coupled diode resonators.

The coupling between the 2 diode resonators is not symmetric, however, and so quasiperiodicity is not present in the single transistor circuit. The coupling is actually rather complex and nonlinear, depending on the voltages across the transistors, so it is not easy to write the equations for this system (eq. 1-4) as 2 diode resonators with coupling. There do exist in this system however forms of chaos that superficially resemble quasiperiodicity, in that the dominant frequency in the chaotic state is not related to the driving frequency by any integer.

In Figure 11, the value of the output signal V_2 from the simulation was recorded each time the driving signal V_0 crossed 0, in the positive or

negative direction. The power spectrum of this strobed signal was calculated for a driving amplitude A_0 = 2.0 V and 3 different frequencies: 2.5 MHz (11(a)), 4.5 MHz (11(b)), and 5.125 MHz (11(c)).

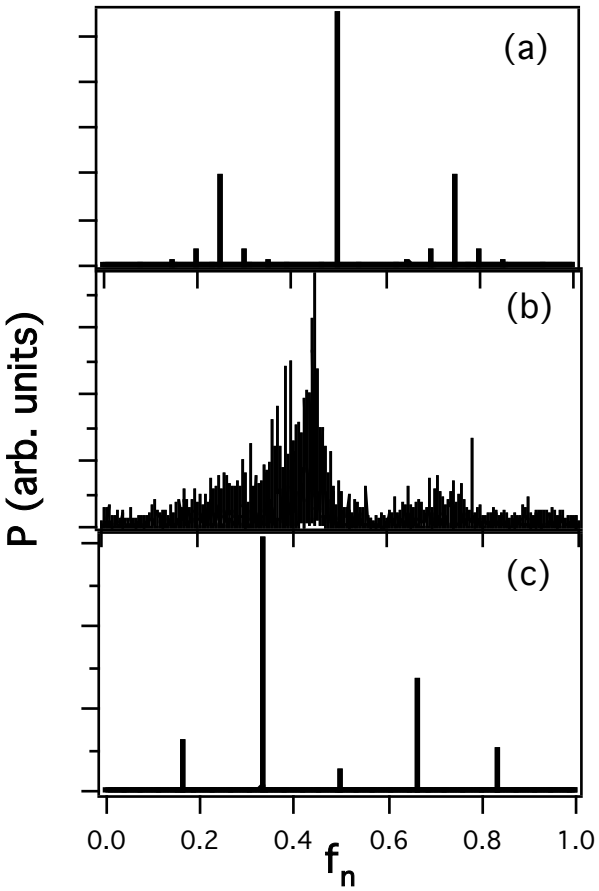

Fig 11. Power spectrum of the strobed V_2 signal from the simulation for a driving amplitude of 2 V. The frequency axis f_n is normalized by the driving frequency. (a) is a period doubled state seen for a driving frequency of 2.5 MHz, (b) is a chaotic state seen for a driving frequency of 4.5 MHz, and (c) is a period 3 state seen for a driving frequency of 5.125 MHz.

Fig 11(a) corresponds to a period doubled state, as can be seen by the large peak at f_n = 0.5, half the driving frequency. Likewise, fig 11(c) shows a period 3 state, with a peak at f_n = 0.33. Fig. 11(b) shows the

strobed spectrum for a chaotic state. The peak frequency in (b) is at f_n = 0.44788, which appears to correspond to a non-integer divisor of the driving frequency. It is when the system is in the chaotic state seen in Fig 11(b) that the low frequency behavior is seen. The transition between Fig. 11(a) and Fig. 11(c) is a period adding transition, which is quite well known [17], except that the standard systems in which the period adding sequence is studied (such as the circle map) do not contain the very broad range of frequencies seen in this work.

Figure 12 a map of the state corresponding to the dominant frequency in the strobed power spectrum for different driving amplitudes and frequencies.

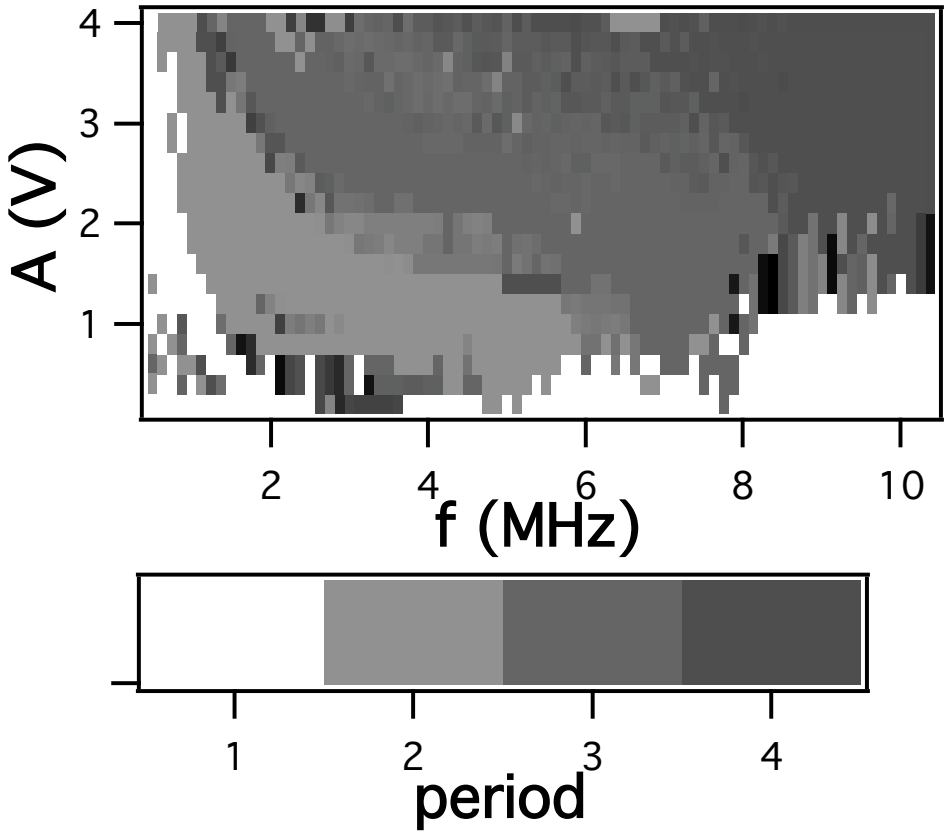

Figure 12. Periodicity of the V_2 signal from the simulation of the single transistor circuit, for different driving amplitudes (A_0) and frequencies.

Fig. 12 shows regions where period 1, 2, 3, or 4 behavior dominates., similar to the standard period adding sequence seen in systems such as the circle map [17]. Unlike the circle map, the chaos seen in the single transistor Schmitt trigger circuit contains frequencies ranging from the driving frequency all the way down to dc.

A more detailed picture may be generated by taking a slice through figs. 10 and 12 at the driving amplitude of 3 V. Figure 13 shows this slice, along with the largest Lyapunov exponent for the simulation.

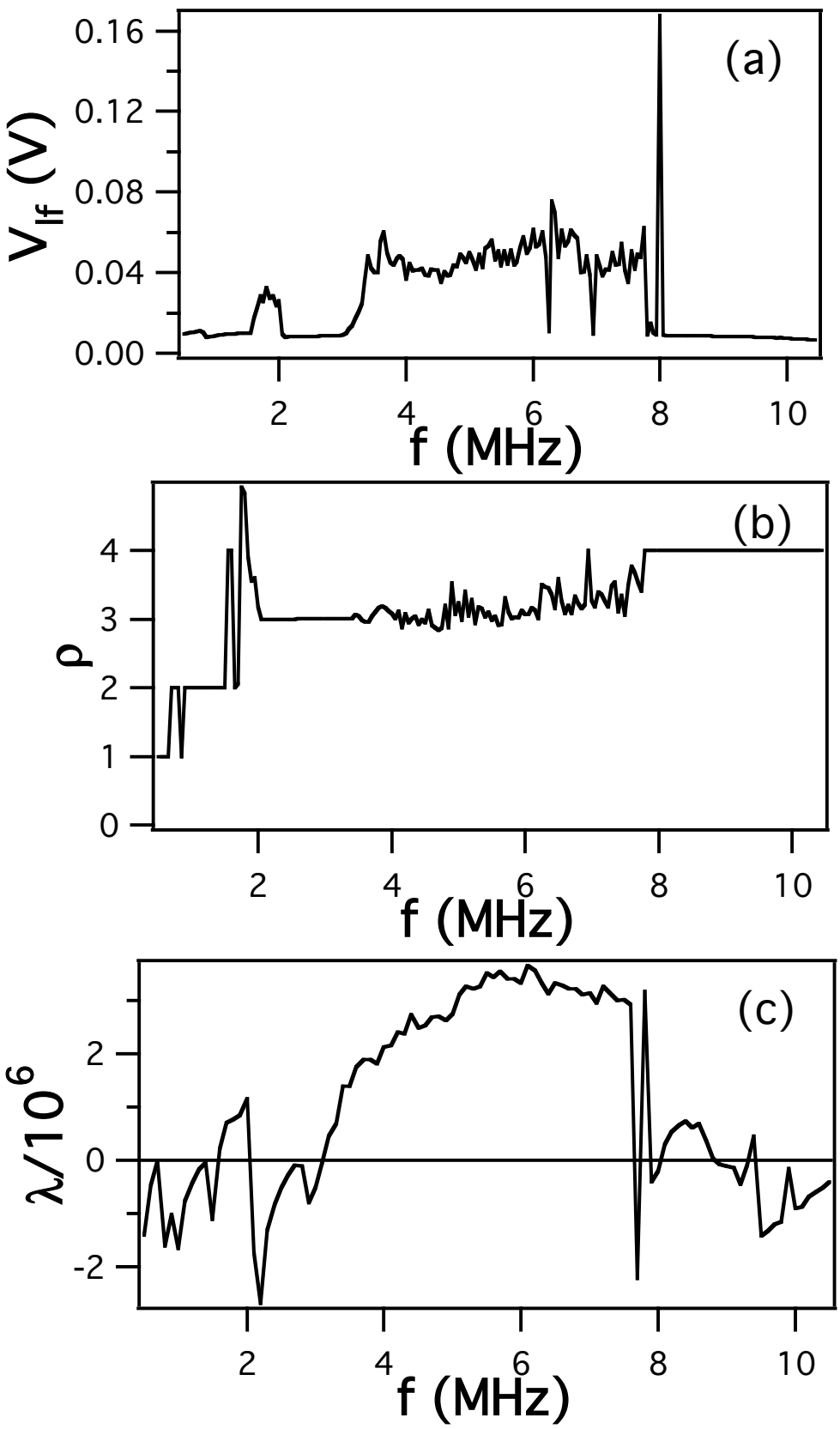
(a)
V_{lf} (V)
0.16
0.12
0.08
0.04
0.00
2
4
6
8
10
f (MHz)
(b)
ρ
4
3
2
1
0
2
4
6
8
10
f (MHz)
(c)
λ/10^6
2
0
-2
2
4
6
8
10
f (MHz)

Fig. 13. (a) shows the rms amplitude of the low pass filtered signal from the simulation of the single transistor circuit, (b) shows the dominant periodicity based on a strobed time series, and (c) shows the largest Lyapunov exponent.

In fig. 13, it can be seen that parameters for which the low frequency signal is large (in 13(a)) correspond to regions where the dominant periodicity does not correspond to a simple integer ratio (13(b)). A similar result was seen for the circuit experiments, although the plot was noisier.. The largest Lyapunov exponent was also calculated and plotted in (c). The Lyapunov exponent shows that the regions of non-integer periodicity (where the large low frequency signal appears) are chaotic, and not quasiperiodic. In a quasiperiodic state, a system has 2 zero Lyapunov exponents [18]. The driving signal V_0 contributes one 0 exponent, but the largest Lyapunov exponent from the model of eqs. (1-4) is never 0 (see fig 13(c)), so at most one Lyapunov exponent is 0, ruling out quasiperiodicity for the single transistor circuit.

Conclusions

The single transistor circuit described in this paper was not much more complicated than the diode resonator, but the dynamics was considerably more complex. Although the original goal was to model a Schmitt trigger, these sort of dynamics could appear in other transistor circuits in which rf energy managed to leak into the power supply leads.

The single transistor circuit above was analogous to a pair of coupled diode resonators. If the resonators are symmetrically coupled, it is

know that quasiperiodicity exists. In this case, the coupling between diode resonators was not symmetric, and a very broad band form of chaos was seen. The chaos in this circuit occurred during period adding transitions, but the chaos in this circuit covered a much broader band of frequencies than the chaos typically seen during a period adding sequence [17]. It seems highly likely that this type of chaos could be rather common, but very few previous researchers have looked at power spectra over such a broad range, so the extremely broad band nature of the chaos was probably not noticed.

References

[1]W. A. Radasky, C. E. Baum, and M. W. Wik, IEEE Transactions on Electromagnetic Compatibility **46**, 314 (2004).

[2]E. R. Hunt and R. W. Rollins, Physical Review A **29**, 1000 (1984).

[3]P. S. Linsay, Physical Review Letters **47**, 1349 (1981).

[4]R. M. d. Moraes and S. M. Anlage, Physical Review E **68**, 26201 (2003).

[5]Z. Su, R. W. Rollins, and E. R. Hunt, Physical Review A **40**, 2698 (1989).

[6]N. Takeuchi, T. Nagai, and T. Matsumoto, Electronics and Communications in Japan **84**, 91 (2001).

[7]S. Tanaka, S. Higuchi, and T. Matsumoto, Physical Review E **54**, 6014 (1996).

[8]J. Testa, J. Perez, and C. Jeffries, Physical Review Letters **48**, 714 (1982).

[9]D. N. Armstead and T. L. Carroll, Physical Review E **71**, 036208 (2005).

[10]T. L. Carroll, Physical Review E **67**, 046208 (2003).

[11]T. L. Carroll, submitted to Chaos (2005).

[12]C. Reick and E. Mosekilde, Physical Review E **52**, 1418 (1995).

[13]R. V. Buskirk and C. Jeffries, Physical Review A **31**, 3332 (1985).

[14]U. Tietze and C. Shenk, *Electronic Circuits* (Springer, Berlin, 1991).

[15]M. J. Cooke, *Semiconductor Devices* (Prentice Hall, Englewood Cliffs, 1990).

[16]H. C. Poon and H. K. Gummel, Proceedings of the IEEE **57**, 2181 (1969).

[17]K. Kaneko, Progress of Theoretical Physics **68**, 669 (1982).

[18]C. Grebogi, E. Ott, and J. A. Yorke, Physica D **15**, 354 (1985).